Results in Physics 58 (2024) 107492

Contents lists available at ScienceDirect

Results in Physics

journal homepage: www.elsevier.com/locate/rinp

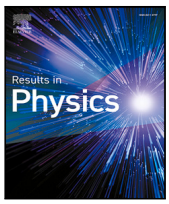

Unveiling the role of MHD forces in Oldroyd 8-constant fluid during Forward roll-coating: Comparing numerical and analytical computations

Muhammad Usman [a], Yanren Hou [a,*], Fateh Ali [b,*], Muhammad Zahid [c], Muhammad Afzal Rana [d]

[a] School of Mathematics & Statistics, Xi'an Jiaotong University, 28 Xianning West Road, Beilin, Xi'an, 710049, Shaanxi, PR China
[b] College of Mathematics and System Sciences, Xinjiang University, 666 Shengli Rd, Tianshan District, Ürümqi, 830049, Xinjiang, PR China
[c] Department of Mathematics, COMSATS University Islamabad, Abbottabad Campus, Abbottabad, 22060, Khyber Pakhtunkhwa, Pakistan
[d] Department of Mathematics & Statistics, Riphah International University, Sector I-14, Islamabad, 44000, Islamabad, Pakistan

ARTICLE INFO

Keywords:
Oldroyd 8-constant fluid
Forward roll coating
Adomian decomposition method
Homotopy analysis method
Finite difference method

ABSTRACT

In this article, the rheological effects of an Oldroyd 8-constant fluid model in the presence and absence of magnetic force (MHD) are investigated while traveling between the two rolls rotates in the same direction. The governing equations of the fluid flow have been simplified using the lubrication approximation theory (LAT). Analytical solutions in the presence and absence of MHD are presented using (i) Adomian's decomposition method (ADM), (ii) Homotopy analysis method (HAM), and numerical simulations are performed by (iii) the finite difference method. We present the results of our findings through various graphs and validate the numerical and analytical methods through detailed tables of error comparisons. It has been found that non-Newtonian and magnetic parameters have a significant impact on the velocity profiles, pressure gradient, pressure distribution, separation points, and coating thickness. The material parameters α_1 (dilatant parameter) and α_2 (pseudoplastic parameter) notably affect the velocity profile of the fluid flow between two rolls. Increasing α_1 causes shear thickening and decreases the velocity profile, while increasing α_2 results in shear thinning and increases the velocity profile due to diminished internal resistance. A relationship exists between the MHD parameter m and the flow velocity. The greater the MHD force, the higher the resistance in fluid flow, resulting in lower velocity. A reasonable agreement has been found between Newtonian fluid and Oldroyd 8-constant fluid, assuming all the non-Newtonian parameters to be zero. The results provided a comprehensive methodology for regulating the coating thickness by adjusting the modified Capillary's number in the industry.

Introduction

Classical Navier–Stokes theory is inadequate for describing rheologically complex fluids, leading to the need for non-Newtonian fluid theories. Researchers are increasingly interested in understanding non-Newtonian fluids, which are commonly used in numerous industrial, medical, and engineering applications, such as blood, drilling operations, petroleum engineering, soap solutions, cosmetics, paint thinners, crude oils, sludge, metals, polymers, and many more. The use of non-Newtonian fluids in the coating industry is undoubtedly useful in creating a uniform thin liquid film over a substrate. Various rheological models are used to represent the relationship between the rate of deformation tensor and stress. These fluid models include Jeffrey, Sisko, Casson, differential types fluid models, different types of grade n [1] fluids, including Phan Thien and Tanner, third and fourth grade, Maxwell, Oldroyd's family, elastic-viscous, power-law, and viscous fluids. Mathematicians study non-Newtonian fluids in depth using differential equation theory to come up with solutions that help engineers make coated materials with the best parameters. The non-linear characteristics of non-Newtonian fluids pose challenges for obtaining solutions through analytical, numerical, or computational methods.

The conservation of mass and linear momentum are the fundamental governing equations of physical systems. To formulate the governing equations based on the physics of the problem, the momentum equation is altered by incorporating the stress tensor derived from the constitutive equation. The lubrication approximation method (LAT) is used to simplify the system of equations. Based on the formulated problem, the boundary conditions that are required have been applied appropriately. The optimal homotopy analysis method (OHAM), the variational iteration method (VIM), and the homotopy perturbation method (HPM) are some methods that have been proposed and studied in the literature to solve such problems. The article discusses analytical solutions using Adomian's decomposition method (ADM), homotopy

* Corresponding authors.
E-mail addresses: muhammadusman@stu.xjtu.edu.cn (M. Usman), yrhou@mail.xjtu.edu.cn (Y. Hou), fatehalirana@xju.edu.cn (F. Ali).

https://doi.org/10.1016/j.rinp.2024.107492
Received 25 November 2023; Received in revised form 4 February 2024; Accepted 18 February 2024
Available online 19 February 2024

analysis method (HAM), and numerical by finite difference method (FDM).

Roll coating is a technique used to apply homogeneous, thin liquid coats to different surfaces, including wallpapers, tenacious video tapes, books, plastic wraps, fabric protectors, X-ray & photographic films, cosmetics, carpets, and foils. Roll coating has gained significant attention in both research and industry recently. A range of instruments and techniques are employed in the coating industry includes roll, wire, blade, and dip coatings. In roll coating process, the substrate must pass between two or multiple rolls with different roll characteristics, such as diameter, speed, etc. Experimental, theoretical, computational, and numerical investigations have all contributed to a greater understanding of the engineering parameters and fluid dynamics incorporated into the various roll coating processes that have been the subject of research advancements. Roll coating can be categorized into metering (MRC), forward (FRC), and reverse roll coating (RRC). Hintermaier and White [2] conducted research on the water flow between two rolls. Their conclusions, aligned with their experiments, were confirmed by the lubricating principle. Greener and Middleman [3] created excellent models based on the concept of lubrication theory that disregarded the benefits of face pressure and vacuity. A three-dimensional model for non-Newtonian fluid flow of the reverse roll-coating process was created by Jang and Chen [4] using the volume of fluids (VoF) free face and finite volume (FVM) approaches, and their research mainly focused on studying inelastic non-Newtonian fluids. Balzarotti and Rosen [5] concluded that when the diameter of the rotating rollers is considerably larger than the gap between these; controls the thickness and uniformity of the applied liquid film. The thickness of the coating is significantly influenced by the rollers and their speed [6]. In the literature, along with several other non-Newtonian fluid models, the Oldroyd 8-constant has been put forward to describe the flow behavior of fluids with distinct rheological properties, and it comprises a number of other fluids as limiting instances. These models cover fluids of the differential, rate, integral, and shear thickening as well as shear thinning types. Hayat et al. [7] has researched the Oldroyd 8-constant fluid in a finite domain to obtain the analytical solution using the homotopy analysis method (HAM). Ellahi et al. [8] researched the nonlinear slip conditions for the Oldroyd 8-constant fluid. For three significant flows (including Poiseuille, Couette, and generalized Couette), the precise solution has been found and is thoroughly explored. S. [9] conduted a research on Oldroyd 8-constant fluid in a convergant channel. With such extensive use, the forward roll coating technique for the investigation is taking into consideration the Oldroyd 8-constant fluid. The applications of the forward roll coating idea with non-Newtonian fluid in industrial, polymer processes, and extrusion systems are the driving force behind this consideration. The nip of the two rolls behaves similarly in FRC. Usman et al. [10,11] utilized the LAT to produce analytical results of viscoelastic and Oldroyd 4-constant fluids using soft computing during the forward roll coating process. Zahid et al. [12] statistically discussed the Rabinowitz fluid. Daprà and Scarpi [13] considered the physical engineering parameters flow rate, roll temperatures, web coating thickness, separation location, force, and stress distribution. Zahid et al. [14] made a contribution to the flow of a porous moving web by using the roll coating process in viscoelastic material.

Magnetohydrodynamics (MHD) is an intriguing subject of study related to materials that transmit electricity. Applications for magnetic force include astrophysics, magnetoacoustics, thermal systems, magnetic equipment, industrial processes, etc. Sarpkaya [15] was the pioneer in the study of non-Newtonian fluids in the presence of the magnetic field. Hayat and Sajid [16] discovered a mathematical solution for the MHD flow of the Upper Convected Maxwell fluid. Also, the same author investigated the MHD flows of an Oldroyd 8-constant fluid with porosity [17]. Khan et al. [18] used a finite differences method and an iterative technique to explore the numerical MHD flow of an Oldroyd 8-constant fluid under the influence of partial slip boundary conditions. An analytical non-linear flow solution has been found for the Oldroyd 8-constant fluid by Ellahi et al. [19]. In the recent studies Hamid et al. [20] studied the impact of Hall current and homogeneous and heterogeneous reactions on MHD flow of GO-MoS2/water (H2O)-ethylene glycol (C2H6O2) hybrid nanofluid past a vertical stretching surface and concluded that the thermal profile declines near convectively heated surface and upsurges away from the surface for incline in mixed convection parameter. The Biot number and volume fraction act as controlling parameters. Raza et al. [21] studied the fractional model for the kerosene oil and water-based Casson nanofluid with inclined magnetic force and observed the enhancement in heat transfer is comparatively higher for the water-based nanofluid as compared to kerosene oil-based nanofluid. Raja et al. [22] conducted a research on the dynamics of entropy optimized nanofluidic system under impacts of MHD along thick surface via artificial Levenberg–Marquardt back propagated neural networks. The purpose of the current research is to develop a mathematical framework for MHD Oldroyd 8-constant fluid during the forward roll coating mechanism. The minuscule space created by two forward coating rollers covers a thin layer of pseudoplastic material. Many researchers have focused on the variety of non-Newtonian fluids with MHD, thermal radiation effects, energy dissipation, and heat transfer over the stretching sheets and coating process. These researchers have used analytical and numerical methods to examine the impact of the physical parameters, heat, entropy, energy, and MHD on the velocity field. This emphasis can also be seen in the literature [23–30].

The current article deals with the mathematical formulation of the governing equations in the next section. The problem formulation section describes the physics of the proposed problem, and the modeled equation is then converted into dimensionless form and applying relevant boundary conditions. Finally, simplifications are carried out using LAT. In the section on the solution of the problem, the detailed solutions are presented. The solution uses MATLAB® and Maple® software to deal with analytical and numerical approaches. Adomian's decomposition method (ADM) [31–35], Homotopy analysis method (HAM) [36,37], and numerical via finite difference method (FDM) are subjected to achieve the analytical and numerical solutions of the resulting nonlinear differential equation for MHD and non-MHD instances. The impact of physical parameters on velocity, pressure gradients, pressure profiles, coating thickness, and separation points was then interpreted using a parametric approach in the results and discussion section. According to the study, physical and MHD factors are vital for regulating pressure distributions and velocity profiles. The coating thickness can be controlled by adjusting the modified Capillary's number. It is asserted that the analytical and numerical results exhibit excellent agreement. To support the claim of comparing various methodologies, an in-depth investigation of the findings has been carried out, integrating detailed graphs and tables. Furthermore, comprehensive conclusions are offered based on the findings. More interpreted results as well as an analysis of the methods and algorithm under study are given in the *Appendix*. According to the authors' knowledge, no prior studies have been done on the governing equations for the steady magnetohydrodynamic (MHD) flow of an Oldroyd 8-constant fluid.

Governing equations

In this article, the motion of an electrically conducting fluid is investigated. The conservation principles of mass and momentum regulate the steady-state flow of the conducting fluid in the Cartesian coordinate system and are governed by:

$$\rho(\mathbf{V}\cdot\nabla)\mathbf{V} = \nabla\cdot\mathbf{T} + \mathbf{J}\times\mathbf{B}, \tag{1}$$

$$div\mathbf{V} = 0, \tag{2}$$

the velocity vector is represented by $\mathbf{V} = (u, 0, 0)$, the current density is represented $\mathbf{J}$, the density is expressed as ρ, and the total magnetic field

is denoted by $\mathbf{B}$, and the total magnetic field is expressed as $\mathbf{B} = \mathbf{B_0} + \mathbf{b}$, where b represents the induced magnetic field. The Maxwell equations and the generalized Ohm's law are implemented in the absence of consideration for displacement currents.

$$\begin{aligned} &\nabla \cdot \mathbf{B} = 0, \\ &\nabla \times \mathbf{B} = \mu_m \mathbf{J}, \\ &\nabla \times \mathbf{E} = 0, \end{aligned} \tag{3}$$

$$\mathbf{J} = \sigma(\mathbf{E} + \mathbf{V} \times \mathbf{B}), \tag{4}$$

where σ is the electric conductivity, μ_m is the magnetic permeability, and $\mathbf{E}$ is the electric field.

The following are the underlying assumptions:

- Across the entire flow field, the values of ρ, μ_m, and σ remain constant.
- The magnetic field $\mathbf{B}$ and velocity field $\mathbf{V}$ are perpendicular, and compared to the imposed magnetic field, the induced magnetic field b is negligible, resulting in a low magnetic Reynolds number [38].
- The existence of an electric field is considered to be absent.

Based on the assumptions mentioned earlier, the electromagnetic body force described in Eq. (1) takes on the following form:

$$(\mathbf{J} \times \mathbf{B}) = \sigma \left[\mathbf{B_0}(\mathbf{V} \cdot \mathbf{B_0} - \mathbf{V}(\mathbf{B_0} \cdot \mathbf{B_0})\right] = -\sigma {B_0}^2 \mathbf{V}. \tag{5}$$

The Cauchy stress tensor, denoted by $\mathbf{T}$ [39,40], for an Oldroyd 8-constant fluid can be defined as follows:

$$\mathbf{T} = -p_1 \mathbf{I} + \mathbf{S}, \tag{6}$$

in which p_1 represents pressure, $\mathbf{S}$ is the extra stress, and $\mathbf{I}$ denotes identity tensor, yields

$$\begin{aligned} &\mathbf{S} + \lambda_1 \frac{D\mathbf{S}}{Dt} + \frac{\lambda_3}{2}(\mathbf{S}\mathbf{A_1} + \mathbf{A_1}\mathbf{S}) + \frac{\lambda_5}{2}(tr\mathbf{S})\mathbf{A_1} + \frac{\lambda_6}{2}[tr(\mathbf{S}\mathbf{A_1})]\mathbf{I} \\ &= \mu \left[\mathbf{A_1} + \lambda_2 \frac{D\mathbf{A_1}}{Dt} + \lambda_4 \mathbf{A_1}^2 + \frac{\lambda_7}{2}[tr(\mathbf{A_1}^2)]\mathbf{I}\right], \end{aligned} \tag{7}$$

$$\mathbf{A_1} = \mathbf{L} + \mathbf{L}^T, \quad \mathbf{L} = grad\mathbf{V}, \tag{8}$$

where the first Rivlin–Ericksen tensor is $\mathbf{A_1}$, the material constants are μ, $\lambda_i (i = 1 \ldots 7)$, and the contravariant convected derivative for steady flow is $\frac{D}{Dt}$ is as follows:

$$\frac{D\mathbf{S}}{Dt} = (\mathbf{V} \cdot \mathbf{V})\mathbf{S} - \mathbf{S}\mathbf{L}^T - \mathbf{L}\mathbf{S}. \tag{9}$$

The velocity and the stress tensor are represented as:

$$\mathbf{V}(y) = \begin{pmatrix} u \\ 0 \\ 0 \end{pmatrix}, \quad \mathbf{S}(y) = \begin{pmatrix} S_{xx} & S_{xy} & S_{xz} \\ S_{yx} & S_{yy} & S_{yz} \\ S_{zx} & S_{zy} & S_{zz} \end{pmatrix}. \tag{10}$$

When Eq. (10) is used, Eq. (2) is precisely attained. Eqs. (1), (5), and (6)–(10) result to the scalar equations shown below:

$$\frac{\partial p_1}{\partial x} = \frac{d}{dy} S_{xy} - \sigma B_0^2 u, \tag{11}$$

$$\frac{\partial p_1}{\partial y} = \frac{d}{dy} S_{yy}, \tag{12}$$

$$\frac{\partial p_1}{\partial z} = \frac{d}{dy} S_{zy}, \tag{13}$$

$$S_{xx} + (\lambda_3 + \lambda_6 - 2\lambda_1) S_{xy} \frac{du}{dy} = \mu(\lambda_4 + \lambda_7 - 2\lambda_2) \left(\frac{du}{dy}\right)^2, \tag{14}$$

$$\begin{aligned} &S_{xy} - \lambda_1 S_{yy} \frac{du}{dy} + \left(\frac{\lambda_3 + \lambda_5}{2}\right)(S_{xx} + S_{yy}) \frac{du}{dy} \\ &\quad + \frac{\lambda_5}{2} S_{zz} \frac{du}{dy} = \mu \frac{du}{dy}, \end{aligned} \tag{15}$$

$$S_{zx} + \left(\frac{\lambda_3 - 2\lambda_1}{2}\right) S_{zy} \frac{du}{dy} = 0, \tag{16}$$

$$S_{yy} + (\lambda_3 + \lambda_6) S_{xy} \frac{du}{dy} = \mu(\lambda_4 + \lambda_7) \left(\frac{du}{dy}\right)^2, \tag{17}$$

$$S_{zy} + \frac{\lambda_3}{2} S_{zx} \frac{du}{dy} = 0, \tag{18}$$

$$S_{zz} + \lambda_6 S_{xy} \frac{du}{dy} = \mu \lambda_7 \left(\frac{du}{dy}\right)^2, \tag{19}$$

$$S_{xx} + S_{yy} = 2\mu(\lambda_4 + \lambda_7 - \lambda_2) \left(\frac{du}{dy}\right)^2 - 2(\lambda_3 + \lambda_6 - \lambda_1) S_{xy} \frac{du}{dy}. \tag{20}$$

By utilizing Eqs. (16) and (18), we have

$$S_{zx} = S_{zy} = 0. \tag{21}$$

Using Eqs. (13), (15), (19), and (21), we obtain

$$\frac{\partial p_1}{\partial z} = 0, \tag{22}$$

$$\begin{aligned} &S_{xy} - \lambda_1 S_{yy} \frac{du}{dy} + \left(\frac{\lambda_3 + \lambda_5}{2}\right)(S_{xx} + S_{yy}) \frac{du}{dy} \\ &\quad - \frac{\lambda_5 \lambda_6}{2} S_{xy} \left(\frac{du}{dy}\right)^2 + \frac{\mu \lambda_5 \lambda_7}{2} \left(\frac{du}{dy}\right)^3 = \mu \frac{du}{dy}. \end{aligned} \tag{23}$$

Taking

$$\hat{p} = p_1 - S_{yy}, \tag{24}$$

using Eqs. (11), (12) and (22), we can write:

$$\frac{\partial \hat{p}}{\partial x} = \frac{d}{dy} S_{xy} - \sigma B_0^2 u, \tag{25}$$

$$\frac{\partial \hat{p}}{\partial y} = \frac{\partial \hat{p}}{\partial z} = 0. \tag{26}$$

We observe from Eq. (26) that $\hat{p} = \hat{p}(x)$ only, and independent of y and z. Therefore, Eq. (25) becomes:

$$\frac{d\hat{p}}{dx} = \frac{d}{dy} S_{xy} - \sigma B_0^2 u. \tag{27}$$

Using Eqs. (14) to (17), (20) and (23) we get:

$$S_{xx} = \frac{1}{M} \left\{ \begin{aligned} &\mu[(\lambda_4 + \lambda_7) - (\lambda_3 + \lambda_6) + 2(\lambda_1 - \lambda_2)] \left(\frac{du}{dy}\right)^2 \\ &+ \mu[\lambda_4 + \lambda_7)\alpha_2 - \alpha_1(\lambda_3 + \lambda_6) \\ &+ 2(\alpha_1 \lambda_1 + \alpha_2 \lambda_2)] \left(\frac{du}{dy}\right)^4 \end{aligned} \right\}, \tag{28}$$

$$S_{xy} = \frac{1}{M} \left\{ \mu \frac{du}{dy} + \mu \alpha_1 \left(\frac{du}{dy}\right)^3 \right\}, \tag{29}$$

$$S_{yy} = \frac{1}{M} \left\{ \begin{aligned} &\mu[-(\lambda_3 + \lambda_6) + (\lambda_4 + \lambda_7)] \left(\frac{du}{dy}\right)^2 \\ &+ \mu[-\alpha_1(\lambda_3 + \lambda_6) + \alpha_2(\lambda_4 + \lambda_7)] \left(\frac{du}{dy}\right)^4 \end{aligned} \right\}. \tag{30}$$

In the equations mentioned above:

$$\alpha_1 = \lambda_1(\lambda_4 + \lambda_7) - (\lambda_4 + \lambda_7 - \lambda_2)(\lambda_3 + \lambda_5) - \frac{\lambda_5 \lambda_7}{2}, \tag{31}$$

$$\alpha_2 = \lambda_1(\lambda_3 + \lambda_6) - (\lambda_3 + \lambda_6 - \lambda_1)(\lambda_3 + \lambda_5) - \frac{\lambda_5 \lambda_6}{2}, \tag{32}$$

$$M = 1 + \alpha_2 \left(\frac{du}{dy}\right)^2. \tag{33}$$

By utilizing the Eq. (29) in Eq. (27), a nonlinear differential equation can be derived in the following manner:

$$\begin{aligned} &\frac{d^2u}{dy^2} + \left[(3\alpha_1 - \alpha_2) + \alpha_1 \alpha_2 \left(\frac{du}{dy}\right)^2\right] \left(\frac{du}{dy}\right)^2 \frac{d^2u}{dy^2} \\ &\quad - \frac{1}{\mu} \left(\sigma B_0^2 u + \frac{d\hat{p}}{dx}\right) \left[1 + \alpha_2 \left(\frac{du}{dy}\right)^2\right]^2 = 0. \end{aligned} \tag{34}$$

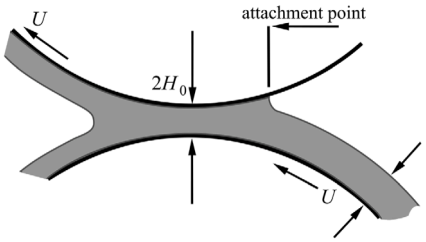

Fig. 1. Schematic representation of the forward roll-coating process (FRC).

Problem formulation

Consider the steady flow of an incompressible fluid with an Oldroyd 8-constant between two rolls that are rotating in the same direction. Fig. 1 depicts the geometric representation of the forward roll coating process as a two-dimensional flow that takes place in the small area between the rolls and the substrate. The substrate is propelled at a velocity of U in the x-direction as the fluid passes the narrow space between the rolls. The rolls remain set at $y = h(x)$. The minimum gap between rolls is denoted by $2H_0$, and the length between the attachment and detachment points of the roll is denoted as L. By pushing the fluid through the rollers, a uniform coating layer of thickness H is produced.

Fig. 1 demonstrates a close approximation to the free surface, as shown:

The appropriate dimensionless parameters Greener and Middleman [41] are shown as follows:

$$\begin{cases} x^* = \dfrac{x}{\sqrt{H_0 R}}, \; y^* = \dfrac{y}{H_0}, \quad u^* = \dfrac{u}{U}, \quad P^* = \sqrt{\dfrac{H_0}{R}}\dfrac{\hat{p}H_0}{\mu U}, \\ S^*_{xy} = \dfrac{S_{xy}H_0}{\mu U}, \; S^*_{xx} = \dfrac{S_{xx}H_0}{\mu U}, \; S^*_{yy} = \dfrac{S_{yy}H_0}{\mu U}, \\ \alpha^*_1 = \dfrac{\alpha_1}{(H_0/U)^2}, \; \alpha^*_2 = \dfrac{\alpha_2}{(H_0/U)^2}, \; m^{*^2} = \dfrac{\sigma B_0^2}{\mu/H_0}. \end{cases} \tag{35}$$

After substituting all the dimensionless parameters into Eq. (34) and simplifying by removing the (*) symbol, the equation is expressed as

$$\frac{d^2u}{dy^2} + \left[(3\alpha_1 - \alpha_2) + \alpha_1\alpha_2\left(\frac{du}{dy}\right)^2\right]\left(\frac{du}{dy}\right)^2\frac{d^2u}{dy^2} - \left(m^2u + \frac{dP}{dx}\right)\left[1 + \alpha_2\left(\frac{du}{dy}\right)^2\right]^2 = 0. \tag{36}$$

To solve the nonlinear differential equation denoted by Eq. (36), it is necessary to specify the correct boundary conditions, which are

$$\begin{cases} \dfrac{du}{dy} = 0 \quad \text{at} \quad y = 0, \\ u = 1 \quad \text{at} \quad y = h(x), \\ \dfrac{dP}{dx} = p = 0 \quad \text{at} \quad x = -\infty. \end{cases} \tag{37}$$

The distance between the line of symmetry and the roll surface is expressed as a dimensionless value represented by the function $h(x)$. Two further boundary conditions are necessary in order to assess the separation point x_{sp}, which was previously unknown. The separation point on the axis of symmetry became a stagnation point, allowing the following boundary conditions to be specified:

$$u = 0, \qquad y = 0, \qquad x = x_{sp}. \tag{38}$$

The terminal boundary condition sets up a connection between the pressure P and the surface tension, pointing to a force/pressure equilibrium at the separation point x_{sp}.

$$P = -\frac{\gamma}{r} \quad \text{at} \quad x = x_{sp} \quad \text{or} \quad P = -\frac{H_0}{r}\left(N_{Ca_2}\right)^{-1} \quad \text{at} \quad x = x_{sp}. \tag{39}$$

The parameter $N_{Ca_2} = \dfrac{\mu U}{\gamma}\left(\dfrac{R}{H_0}\right)^{\frac{1}{2}}$ represents the modified Capillary's number.

$$2r + 2H = 2H_0 h(x_{sp}),$$

or

$$h_{sp} - \lambda = \frac{r}{H_0}. \tag{40}$$

It is established that $h_{sp} = 1 + \dfrac{x^2}{2}$, expressed as follows:

$$h_{sp} = 1 + \frac{x_{sp}^2}{2}. \tag{41}$$

and

$$\lambda = \frac{H}{H_0}, \tag{42}$$

where the separation points x_{sp} and the dimensionless coating thickness λ, are the important parameters calculated through this model.

Solution of the problem

This section comprises three subsections. The first two subsections deal with the analytical solution, while the third subsection discusses the numerical solution. In the first subsection, Adomian's decomposition method (ADM) is utilized for obtaining the analytical solution. The second subsection delves into homotopy perturbation method (HAM). Numerical results are obtained using the finite difference method in the third subsection. The expressions of the derived analytical results are only available for non-MHD case because other expressions take up much space to write within.

Adomian's Decomposition Method (ADM)

The solution to the non-linear differential equation modeled in Eq. (36), along with the boundary conditions made in Eqs. (37)–(42), will be determined. The analysis of the methodology has been discussed in Appendix A. It should be noted that the convergence of this method has been discussed in a previous study [42].

Zero order solution

The zero-order solution for the nonlinear boundary value problem formulated in Eq. (36) subjected to the suitable boundary condition Eq. (37) is given by:

$$u_0 = 1 + \left(\frac{y^2}{2} - \frac{h^2}{2}\right)\frac{dP_0}{dx}. \tag{43}$$

In Eq. (43), the term $\dfrac{dP_0}{dx}$ is unknown and could be determined by considering the zero-order dimensionless volumetric flow rate of Q_0:

$$Q_0 = \int_0^h (u_0) = \xi_0. \tag{44}$$

By applying Eq. (43) to Eq. (44) and separating for zero-order pressure gradient, we get:

$$\frac{dP_0}{dx} = \left(-\frac{3\left(\xi_0 - h\right)}{h^3}\right), \tag{45}$$

integrating the Eq. (45) and boundary condition yields the zero-order pressure distribution

$$P_0(x_{sp}) = -\int_{-\infty}^{x_{sp}}\left(-\frac{3\left(\xi_0 - h\right)}{h^3}\right)dx. \tag{46}$$

By using Eq. (45) into equation. (43), we get

$$u_0 = 1 - \frac{3\left(\frac{y^2}{2} - \frac{h^2}{2}\right)(\xi_0 - h)}{h^3}, \tag{47}$$

by substituting the conditions provided in Eq. (38) into Eq. (47), we obtain

$$1-\frac{3}{2}\frac{(\xi_0-h_1)}{h_1^3}\left(-h_1^2\right)=0, \tag{48}$$

declaring $h_1(x)$ as:

$$h_1=3\xi_0. \tag{49}$$

Also for $x=x_1$, will become

$$1-\frac{3}{2}\frac{(\xi_0-h_1(x))}{h_1^3(x)}\left(-h_1^2(x)\right)=0. \tag{50}$$

Since

$$h_1(x_1)=1+\frac{x_1^2}{2}, \tag{51}$$

by use of $h_1(x_1)$ in Eq. (45), the relation in term of x_1 is expressed as:

$$x_1=\left[2\left(3\xi_0-1\right)\right]^{\frac{1}{2}}. \tag{52}$$

The final boundary condition indicates that there is pressure on the separation point at x_1. The pressure P can be related to the surface tension γ.

$$P=-\frac{\gamma}{r}\quad \text{at}\quad x=x_1,$$

or

$$P=-\frac{H_0}{r}\left(N_{Ca_2}\right)^{-1}\quad \text{at}\quad x=x_1.$$

The modified capillary number N_{Ca_2} can be used to express the zero-order pressure distribution at $x=x_1$.

$$P_0(x_1)=-\frac{1}{\left(h_1-\lambda_0\right)N_{Ca_2}}=-\int_{-\infty}^{x_1}\left(-\frac{3\left(\xi_0-h\right)}{h^3}\right)dx. \tag{53}$$

The zero-order solution acquired in this particular section corresponds to the Middleman Greener and Middleman [41] for both the detachment point and the velocity distribution.

First order solution

The first-order solution can be assessed by employing Eqs. (73) and (74)

$$u_1=\left(\frac{y^6}{6}-\frac{h^6}{6}\right)l_1+\left(\frac{y^4}{4}-\frac{h^4}{4}\right)l_2+\left(\frac{y^2}{2}-\frac{h^2}{2}\right)\frac{dP_1}{dx}, \tag{54}$$

In Eq. (54), the term $\frac{dP_1}{dx}$ is still not known and can be determined by calculating the dimensionless volumetric flow rate Q_1 in a manner comparable to zero order:

$$Q_1=\int_0^h(u_1)=\xi_1, \tag{55}$$

$$\xi_1=\frac{1}{7}l_4h^7+\frac{1}{5}l_3h^5-\frac{1}{3}\frac{dP_1}{dx}h^3-\frac{1}{6}l_1h^7-\frac{1}{4}l_2h^5. \tag{56}$$

To set up the pressure gradient of first-order, we can use Eq. (55) in Eq. (56),

$$\frac{dP_1}{dx}=-\frac{h^4l_1}{2}-\frac{3h^2l_2}{4}-\frac{3}{h^3}\left(\xi l_1-\frac{1}{7}l_4h^7-\frac{1}{5}l_3h^5\right). \tag{57}$$

By substituting the expression for the pressure gradient of first-order from Eq. (57) to Eq. (54), the solution can be written as:

$$\begin{aligned}u_1=&\left(\frac{1}{6}y^6-\frac{1}{4}h^4y^2+\frac{1}{12}h^6\right)l_1+\left(\frac{1}{4}y^4-\frac{3}{8}h^2y^2+\frac{1}{8}h^4\right)l_2\\&+\left(\frac{3}{10}h^2y^2-\frac{3}{10}h^4\right)l_3+\left(\frac{3}{14}h^4y^2-\frac{3}{14}h^6\right)l_4\\&-\frac{3\xi l_1y^2}{2h^3}+\frac{3\xi l_1}{2h}.\end{aligned} \tag{58}$$

By incorporating the conditions from Eq. (38), into the velocity equation, one can obtain an approximation of the coating thickness as follows:

$$\frac{l_1h^6}{12}+\frac{l_2h^4}{8}-\frac{3h^4l_3}{10}-\frac{3h^6l_4}{14}+\frac{3\xi_1}{2h}=0, \tag{59}$$

inserting $h=1+\frac{x^2}{2}$, the expression for first-order coating thickness is obtained

$$\begin{aligned}\xi_1=&\frac{9\left(x^2-2\xi_0+2\right)^3\left(-\alpha_2+\alpha_1\right)}{5\left(x^2+2\right)^8}\left(x^8+8x^6+\left(\frac{48\alpha_2}{7}+24\right)x^4\right.\\&\left.+16+\left(32+\left(-\frac{192\xi_0}{7}+\frac{192}{7}\right)\alpha_2\right)x^2+\frac{192\left(\xi_0-1\right)^2\alpha_2}{7}\right).\end{aligned} \tag{60}$$

where l_1,l_2,l_3 and l_4 are constant containing the auxiliary constants also are given in . We obtained an approximate second-order solution by combining zeroth order (Eq. (47)) and first order (Eq. (58)) of the velocity field in Eq. (78). Due to lengthy expressions obtained for the second component, only the graphical representation up to the second-order approximation is presented.

Homotopy Analysis Method (HAM)

Based on the methodology presented in Appendix B, the second-order approximation solution for the non-linear differential Eq. (36) together with suitable boundary conditions in Eq. (37) for non-MHD case can be computed as:

$$u_0=\frac{1}{2}\mathcal{P}y^2+1-\frac{1}{2}\mathcal{P}h^2, \tag{61}$$

$$u_1=\hbar\begin{bmatrix}\frac{1}{30}\mathcal{P}^5\alpha_1\alpha_2y^6-\frac{1}{12}\mathcal{P}^3\beta y^4+\frac{1}{2}y^2\left(\mathcal{P}^2\alpha_2+1\right)^2\mathcal{P}\\-\frac{1}{2}\mathcal{P}y^2+\frac{1}{30}\mathcal{P}^5\alpha_1\alpha_2h^6-\frac{1}{2}\mathcal{P}^5h^2\alpha_2^2\\+\frac{1}{12}\mathcal{P}^3\beta h^4-\mathcal{P}^3h^2\alpha_2\end{bmatrix}, \tag{62}$$

$$u_2=\frac{\hbar^2}{2!}\begin{bmatrix}\frac{1}{50}\mathcal{P}^9\alpha_1^2\alpha_2^2x^{10}+\frac{1}{15}\mathcal{P}^7\beta\alpha_1\alpha_2x^8-\frac{7}{15}\mathcal{P}^7x^6\alpha_2^2\alpha_1\\-\frac{3}{10}\mathcal{P}^9x^6\alpha_2^3\alpha_1+\frac{1}{18}\mathcal{P}^5\beta x^6-\frac{7}{12}\mathcal{P}^7x^4\alpha_2^2\beta\\-\frac{5}{6}\mathcal{P}^5x^4\beta\alpha_2+4\mathcal{P}^5x^2\alpha_2^2+6\mathcal{P}^7x^2\alpha_2^3+2\mathcal{P}^9x^2\alpha_2^4\\-\frac{1}{50}\mathcal{P}^9\alpha_1^2\alpha_2^2h^{10}+\frac{3}{10}\mathcal{P}^9h^6\alpha_2^3\alpha_1-\frac{1}{15}\mathcal{P}^7\beta\alpha_1\alpha_2h^8\\+\frac{7}{15}\mathcal{P}^7h^6\alpha_2^2\alpha_1-2\mathcal{P}^9h^2\alpha_2^4+\frac{7}{12}\mathcal{P}^7h^4\alpha_2^2\beta\\-\frac{1}{18}\mathcal{P}^5\beta h^6-6\mathcal{P}^7h^2\alpha_2^3+\frac{5}{6}\mathcal{P}^5h^4\beta\alpha_2-4\mathcal{P}^5h^2\alpha_2^2\end{bmatrix}, \tag{63}$$

where $\mathcal{P}=\frac{dP}{dx}$ and $\hbar=-0.1$. The solution has been represented as a series given in Eq. (87).

Numerical

We aim to numerically solve the differential equation Eq. (36) with its suitable boundary conditions Eq. (37) using appropriate methods. Due to the non-linearity of the differential Eq. (36), the BVP cannot be solved directly with the finite-difference method. It is common practice to use iterative methods to solve nonlinear equations. An iterative procedure successive under-relaxation (SOR) can be constructed as follows:

$$\begin{aligned}&\frac{d^2u^{(n+1)}}{dy^2}+\left[(3\alpha_1-\alpha_2)+\alpha_1\alpha_2\left(\frac{du^{(n)}}{dy}\right)^2\right]\left(\frac{du^{(n)}}{dy}\right)^2\frac{d^2u^{(n+1)}}{dy^2}\\&\qquad-\left(m^2u^{(n+1)}+\frac{dP}{dx}\right)\left[1+\alpha_2\left(\frac{du^{(n)}}{dy}\right)^2\right]^2=0.\end{aligned} \tag{64}$$

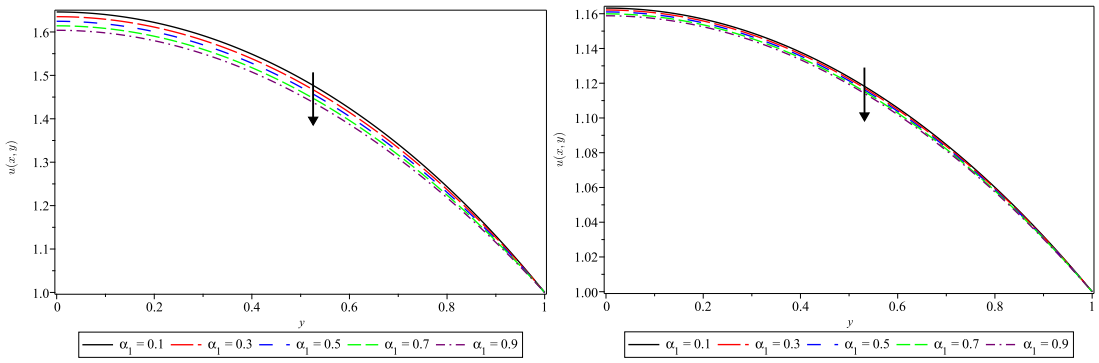

(a) without considering the MHD contribution (b) with considering the MHD contribution

Fig. 2. Non-dimensional velocity profiles at the nip ($x = 0$) for different dilatant parameter values α_1, with constant pseudoplastic parameter α_2.

wherein (n) represents the iterative step. Confirming that Eq. (64) is consistent with Eq. (36) is easy if we remove indices (n) and $(n + 1)$. Eq. (64) and the corresponding boundary conditions are

$$\begin{aligned} \frac{du^{(n+1)}}{dy} &= 0 \quad \text{at} \quad y = 0, \\ u &= U_0 \quad \text{at} \quad y = h(x), \end{aligned} \tag{65}$$

in which $U_0 = 1$, the formulation of the linear differential BVP for $u(n + 1)$. For each iterative step $(n + 1)$, it is possible to derive the discretizated form and solve a linear algebraic equation system using the finite-difference method. Consequently, we establish a sequence of functions $u^{(n)}(y), n = 0, 1, 2, \ldots$ by the subsequent method: if an initial estimation of $u^{(0)}(y)$ is provided, then $u^{(n)}(y), n = 1, 2, \ldots$ are determined respectively as solutions to the boundary value problem posed by the Eqs. (64) and (65).

The method of successive under-relaxation is a popular technique used to improve the convergence of an iterative process. We solve the BVP in Eq. (64) and the boundary condition in Eq. (65) for step $n + 1$ to estimate $u^{(n+1)} : \tilde{u}^{(n+1)}$. Then, the formula defines $u^{(n+1)}$ as

$$u^{(n+1)} = u^{(n)} + \tau(\tilde{u}^{(n+1)} - u^{(n)}), \qquad \tau \in (0, 1]. \tag{66}$$

where $\tau \in (0, 1]$ is a parameter for under-relaxation. To ensure convergence, we need to select a small value for τ and iterate until it converges. The iterative procedure ought to continue until the difference between $u^{(n+1)}$ and $u^{(n)}$ is less than a specified error of 10^{-8}. The algorithm and procedure has been discussed in Appendix C.

Results and discussion

In this current article, the coating material of Oldroyd 8-constant fluid was modeled during the forward roll coating process. The velocity profile is considerably impacted by physical parameters such as the dilatant constant α_1, pseudoplastic constant α_2, pressure gradient $\frac{dP}{dx}$, and magnetic parameter m is shown in Figs. 2 to 8. In Fig. 9, we examine the pressure gradient and pressure profile in the absence of the MHD parameter. Table 1 shows the relation of Capillary's number with separation points x_{sp} and thickness of coated fluid ξ without involving the MHD parameter.

The Adomian's decomposition method (ADM), Homotopy analysis method (HAM), and finite difference method (FDM) were used to obtain analytical and numerical solutions. The FDM followed by successive under-relaxation, was also employed to achieve better convergence. The impact of different parameters on velocity profiles, pressure gradient and pressure distribution are displayed in several graphs. Velocity profiles analyzed at the nip ($x = 0$) and away from the nip ($x = 0.75$) are compared for both analytical and numerical solutions, with and without MHD effects, displayed in Tables 2–11.

Table 1
Separation points x_{sp} and coating thickness ξ at different modified Capillary's Number N_{ca_2}.

N_{ca_2}	x_{sp}	ξ
0.1	5.81232	1.88741
0.2	5.44197	1.65506
0.3	5.26952	1.56395
0.4	5.16347	1.51472
0.5	5.08895	1.48381
0.6	5.03224	1.46261
0.7	4.98669	1.44718
0.8	4.94863	1.43547
0.9	4.91587	1.42631
1	4.88699	1.41893
5	4.41478	1.37209
10	4.33715	1.36692
50	4.28421	1.36245
100	4.27802	1.36182
200	4.27495	1.36153

Effect on physical parameters on velocity profiles

Figs. 2 and 3 shows the impact of the dilatant parameter α_1 varies with the non-dimensional velocity profile for both cases at $x = 0$ and 0.75 respectively. It has been observed that when the dilatant parameter α_1 is increased from $\alpha_1 = 0.1$ to 0.9, the velocity of the fluid is found to decrease the phenomenon of shear thickening has been observed. This is due to increased internal fluid resistance as the flow rate increases. At lower values of α_1, the velocity variation is comparable to the Newtonian case (when $\alpha_1 = \alpha_2$). However, as the value of α_1 increases, velocity profiles are prone to decrease. In Figs. 2(a) and 2(b), the velocity trends seem to be the same for both cases at the nip region, i.e., at $x = 0$ except that for increasing α_1 the velocity profiles are much closer to each other when the MHD parameter is involved. When the flow of the fluid moves away from the nip region and reaches $x = 0.75$, the difference between the velocity profiles for both cases becomes prominent, and the MHD parameter causes the flow to decrease, which will be discussed in Section "Effect of MHD parameter on velocity profiles".

The velocity profiles for both cases at $x = 0$ and 0.75 are shown in Figs. 4 and 5 with the effect of pseudoplastic parameter α_2. It can be observed that the behavior is indicative of an increase in α_2 from 0.1 to 0.9, which is investigated and found to be quite opposite to that of the behavior of α_1. It can be further stated that the dilatant parameter reduces velocity, whereas the pseudoplastic parameter (which describes the melt polymer in an Oldroyd 8-constant fluid) increases velocity and shear thinning phenomenon is observed. This because reduced friction forces at higher flow rates allow for faster movement. The dilatant and pseudoplastic characteristics of the coating fluid can be used to manage the desired quality of coating since the velocity of the coating fluid

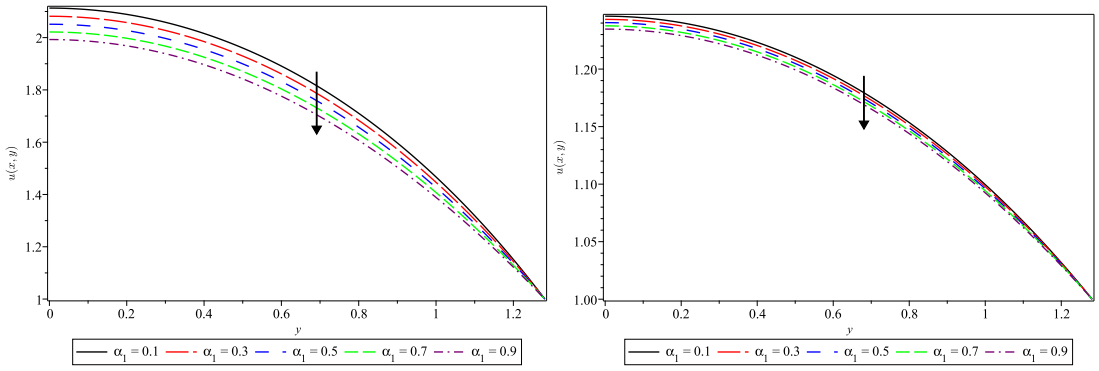

(a) without considering the MHD contribution (b) with considering the MHD contribution

Fig. 3. Non-dimensional velocity profiles away from the nip ($x = 0.75$) for different dilatant parameter values α_1, with constant pseudoplastic parameter α_2.

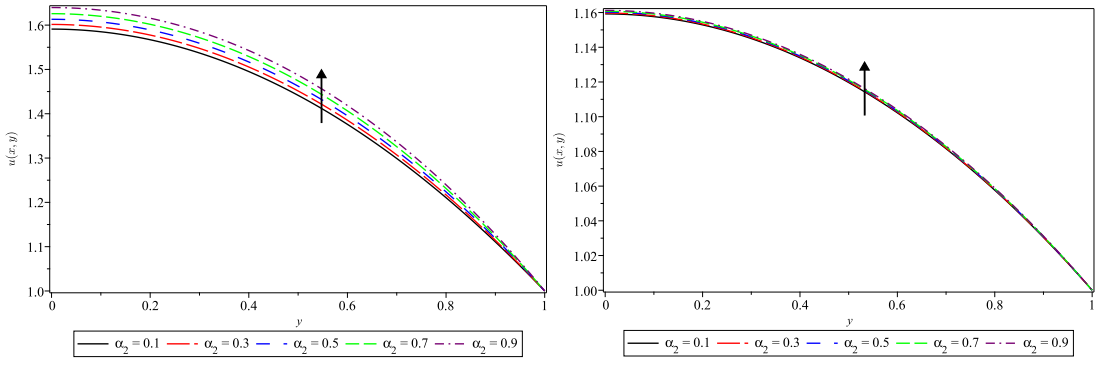

(a) without considering the MHD contribution (b) with considering the MHD contribution

Fig. 4. Non-dimensional velocity profiles at the nip ($x = 0$) for different pseudoplastic parameter values α_2, with constant dilatant parameter α_1.

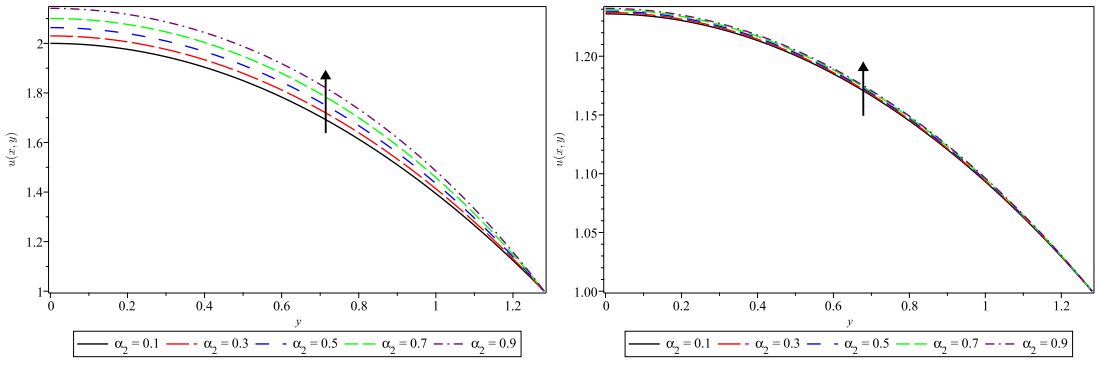

(a) without considering the MHD contribution (b) with considering the MHD contribution

Fig. 5. Non-dimensional velocity profiles away from the nip ($x = 0.75$) for different pseudoplastic parameter values α_2, with constant dilatant parameter α_1.

is a crucial component of design. The coating thickness is observed to increase with increasing dilatant parameter α_1 values; however, the effect of the pseudoplastic parameter α_2 is the opposite. To conclude, we observe that velocity profiles depend on dilatant and pseudoplastic parameters.

Effect of pressure gradient on velocity profiles

The behavior of the velocity profiles has been examined in Figs. 6 and 7 by assuming the dilatant α_1 and pseudoplastic α_2 parameters to be constant with varying pressure gradient $\frac{dP}{dx}$ for non-MHD (Figs. 4(a) and 5(a)) and MHD (Figs. 4(b) and 5(b)) cases at $x = 0$ and 0.75 respectively. When dealing without the MHD parameter, the velocity profiles tend to decrease with increasing pressure gradient. As discussed earlier, the MHD parameter decreases the velocity for dilatant α_1 and pseudoplastic α_2 parameters; the same behavior has been found here, but when the pressure gradient is quite smaller, a bit increase in velocity can be found. The strength of the pressure gradient has a significant impact on the magnitudes of the velocity profiles, and the flow directions are the opposite of the pressure gradient's direction. The flow velocities are significantly higher than those of the Newtonian fluid when α_1 and α_2 are fixed. Nevertheless, this finding is not applicable to other Oldroyd 8-constant fluids with different material parameters.

Effect of MHD parameter on velocity profiles

The implications of the magnetic parameter (MHD) m is demonstrated in Fig. 8 at $x = 0$ and 0.75 (Figs. 8(a) and 8(b)) for the velocity profiles. As the magnetic parameter rises, we note decreases in the

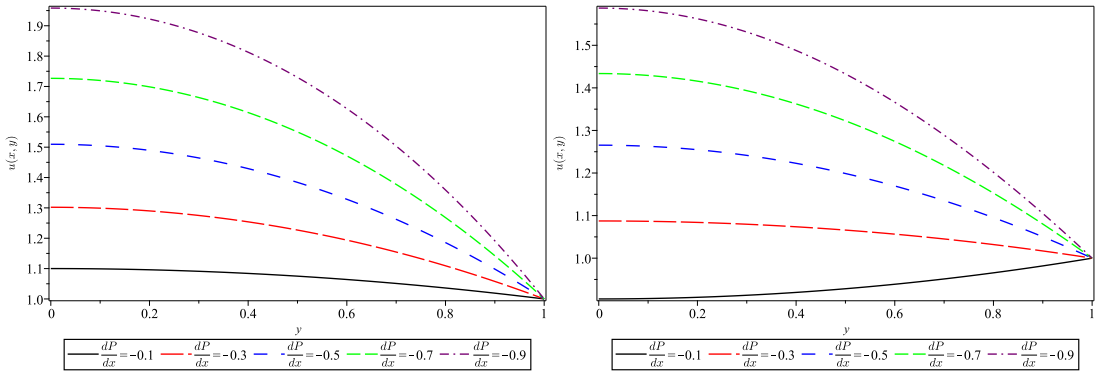

(a) without considering the MHD contribution (b) with considering the MHD contribution

Fig. 6. Non-dimensional velocity profiles for varying pressure gradient values at the nip ($x = 0$) for fixed dilatant α_1 & pseudoplastic parameters α_2.

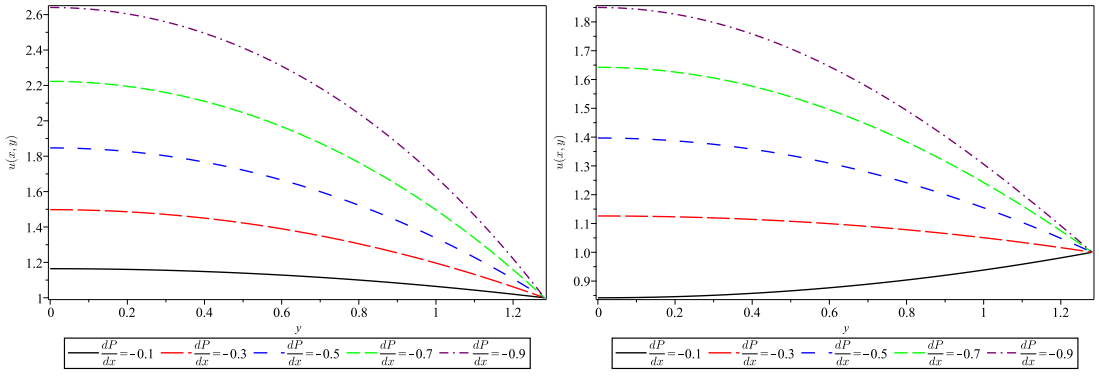

(a) without considering the MHD contribution (b) with considering the MHD contribution

Fig. 7. Non-dimensional velocity profiles for varying pressure gradient $\frac{dP}{dx}$ values away from the nip ($x = 0.75$) for fixed dilatant α_1 & pseudoplastic parameters α_2.

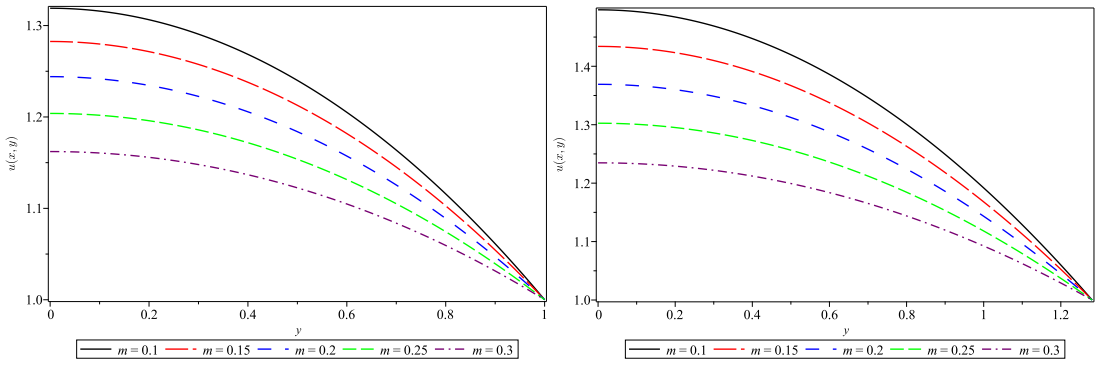

(a) at the nip ($x = 0$) (b) away from the nip ($x = 0.75$)

Fig. 8. Non-dimensional velocity profiles for magnetic forces MHD values for fixed dilatant α_1 & pseudoplastic parameters α_2.

velocity profile and find that there is a prominent change in velocity at the nip region and when the flow of the fluid moves away from the nip region, but there is no significant change in the behavior of the velocity profiles throughout. A higher Lorentz force is generated when the magnetic parameter m is increased, resulting in a corresponding rise in the resistance in the motion of the fluid. It slows down the velocity of the fluid due to this resistance. As the magnetic parameter value increases, the Lorentz force also increases, resulting in a stronger resistance to the fluid's motion and ultimately leading to a reduced fluid velocity.

It is significant to note that if $\alpha_1 = \alpha_2$, an Oldroyd 8-constant fluid exhibits identical behavior to a Newtonian fluid. In addition, when there is no pressure gradient or magnetic parameter, Eq. (36) simplifies to $\frac{d^2u}{dy^2} = 0$ for both types of fluids, resulting in a linear flow velocity. It is conceivable to observe the impact of shear thickening of the non-Newtonian fluid with α_1 varying between 0.1 and 0.9. The Eq. (36) makes it clear that compared to Newtonian fluids, Oldroyd fluids have a greater (smaller) flow velocity if $\alpha_1 < \alpha_2$ ($\alpha_1 > \alpha_2$).

Effect of physical parameters on pressure distributions

Fig. 9 shows the impact of α_1 and α_2 on the pressure gradient and pressure distribution in the absence of MHD parameter. According to the data stipulated, it seems that the pressure gradient decreases as α_1 values increase in the vicinity of the nip region 9(a). The relationship between pressure distribution and distance x is illustrated in the graph presented in Fig. 9(b), providing a detailed insight that as α_1 increases, the pressure P tends to increase in the vicinity of the nip region.

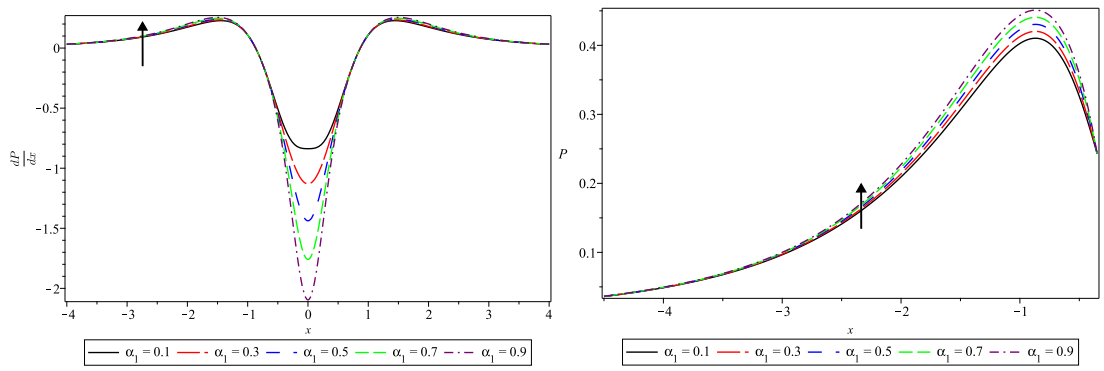

(a) without considering the MHD contribution (b) without considering the MHD contribution

Fig. 9. Non-dimensional (a) pressure gradient $\frac{dP}{dx}$ and (b) pressure P profiles for different dilatant parameter values α_1, with constant pseudoplastic parameter α_2.

Table 2
Validation of numerical model against analytical solution for non-Newtonian flow at $y = 0$ with fixed pseudoplastic parameter α_2 and absence of MHD interaction.

α_1	$x = 0$					$x = 0.75$				
	ADM	HAM	AE	Numerical	AE	ADM	HAM	AE	Numerical	AE
0.1	1.64605	1.64259	3.46×10^{-3}	1.65441	8.36×10^{-3}	2.11298	2.08585	2.71×10^{-2}	2.11583	2.82×10^{-3}
0.3	1.63524	1.63064	4.59×10^{-3}	1.64101	5.77×10^{-3}	2.08167	2.09681	1.51×10^{-2}	2.08641	4.73×10^{-3}
0.5	1.62460	1.61862	5.98×10^{-3}	1.62594	1.34×10^{-3}	2.05118	2.05816	6.97×10^{-3}	2.05232	1.11×10^{-3}
0.7	1.61413	1.60865	5.49×10^{-3}	1.61136	2.77×10^{-3}	2.02152	2.02277	1.25×10^{-3}	2.02845	6.88×10^{-3}
0.9	1.60385	1.59838	5.46×10^{-3}	1.60298	8.73×10^{-4}	1.99266	1.98972	2.95×10^{-3}	1.99071	1.97×10^{-3}

Effect of modified Capillary's number

Table 1 shows that as N_{ca_2} increases, the stronger viscous forces within the fluid make it resist thinning and spreading easily. This translates to a delayed separation pushing the separation point (x_{sp}) closer to the nip ($x = 0$). A closer separation point can be beneficial for achieving thinner coatings, as the fluid has less time to spread before depositing on the substrate. With increasing N_{ca_2}, the fluid's resistance to deformation hinders its spreading on the substrate. This results in a thinner final coating thickness (ξ). These findings highlight the significant influence of the modified Capillary number (N_{ca_2}) on the separation point and coating thickness in forward roll-coating with an Oldroyd 8-constant fluid. By carefully controlling N_{ca_2} through adjusting fluid properties, roller speeds, and other process parameters, you can tune the separation point and achieve desired coating thickness, optimizing the overall coating process.

Validation

The solution to the non-linear differential equation modeled in Eq. (36), along with the boundary conditions made in Eq. (37) has been presented in the previous section in detail. The comparison of the analytical and numerical methods for both cases, i.e., with and without the effect of MHD is necessary to ensure reliability of the discussed methodologies. Tables 2–11 provide a detailed comparison by assigning values to dilatant parameter $\alpha_1 = 0.1, 0.3, 0.5, 0.7, 0.9$ for y from 0 to $y = 0.8$ with a difference of 0.2 at the nip $x = 0$ and away from the nip $x = 0.75$ contain a detailed comparison. The tables present the absolute error of ADM against HAM and numerical methods, demonstrating the convergence of methods. The absolute error was found very promising and ranges from 10^{-2} to 10^{-4}.

It is noteworthy that pseudoplastic parameter α_2 has accelerated impact on the velocity profiles. If we physically increase the pseudoplastic parameter α_2, the friction forces would decrease, resulting in a higher velocity of the fluid. Consequently, it is inferred that the dilatant parameter α_2 and the magnetic parameter (MHD) m both contribute to reducing the velocity of the fluid at any point of the flow domain.

Concluding remarks

This research article examines the steady state flow of an incompressible fluid between two rolls undergoing magnetic field interaction. A nonlinear constitutive model with Oldroyd 8-constant fluid has been employed. The governing equations of the proposed problem were simplified using LAT, non-dimensionalized, and developed into one-dimensional non-linear ordinary differential equation. To analyze the impact of material properties and magnetic field on flows, the nonlinear equation was solved analytically by ADM, HAM and numerically by FDM, followed by the so-called system under the successive over relaxation method. The analytical solutions were compared with the numerical results for the Oldroyd 8-constant fluid to ensure the reliability of the discussed methods. Absolute error are also evaluated in the context of ADM with HAM & numerical method and found good agreement between the comparisons made. We concluded from the study that the profound influence of a magnetic field on fluid movement in roll-coating process is present. As the magnetic field strength increases, a Lorentz force is generated, acting against the fluid flow. This resistance translates to a gradual decrease in velocity. The MHD parameter m effectively captures the interplay between magnetic and fluid forces. Higher m values imply a stronger Lorentz force and, consequently, a more pronounced reduction in velocity. Beyond the magnetic field, the material properties of the fluid also play a crucial role in shaping the velocity profile. Increased α_1 signifies shear thickening, where the fluid's viscosity rises with flow rate. This translates to enhanced internal resistance, leading to a decrease in velocity. In contrast, increasing α_2 triggers shear thinning, where the fluid's viscosity decreases with flow rate. A noticeable disparity exists in flow velocity between Oldroyd 8-constant and Newtonian fluids. If $\alpha_1 < \alpha_2$ (where α_1 is less than α_2), the Newtonian fluid has a lower flow velocity than an Oldroyd 8-constant fluid. In comparison to a Newtonian fluid, if $\alpha_1 > \alpha_2$ (where α_1 is greater than α_2), an Oldroyd 8-constant fluid has a decreased flow velocity. The presented solutions include the Newtonian fluid ($\lambda_i = 0, i = 1, \ldots, 7$), second-grade fluids ($\lambda_i = 0, i = 1, 3, \ldots, 7; \mu\lambda_2 = \alpha_1$ (a material constant of second-grade fluids)), Oldroyd 3-constant fluids ($\lambda_i = 0, i = 3, \ldots, 7$), Oldroyd 6-constant fluids ($\lambda_6 = \lambda_7 = 0$), and Maxwell fluids ($\lambda_i = 0, i = 2, \ldots, 7$) as specific scenarios. The mathematical findings for

Table 3
Validation of numerical model against analytical solution for non-Newtonian flow at $y = 0.2$ with fixed pseudoplastic parameter α_2 and absence of MHD interaction.

α_1	$x = 0$					$x = 0.75$				
	ADM	HAM	AE	Numerical	AE	ADM	HAM	AE	Numerical	AE
0.1	1.62198	1.62693	4.95×10^{-3}	1.62918	7.20×10^{-3}	2.11298	2.08585	2.71×10^{-2}	2.08682	2.11×10^{-3}
0.3	1.61118	1.61358	2.40×10^{-3}	1.61617	4.99×10^{-3}	2.08167	2.09681	1.51×10^{-2}	2.06634	8.68×10^{-3}
0.5	1.60056	1.59861	1.96×10^{-3}	1.60152	9.59×10^{-4}	2.05118	2.05816	6.97×10^{-3}	2.02937	2.15×10^{-3}
0.7	1.59011	1.59264	2.53×10^{-3}	1.58735	2.76×10^{-3}	2.02152	2.02277	1.25×10^{-3}	2.00341	5.90×10^{-3}
0.9	1.57984	1.58012	2.81×10^{-4}	1.57916	6.77×10^{-4}	1.99266	1.98972	2.95×10^{-3}	1.96581	2.86×10^{-3}

Table 4
Validation of numerical model against analytical solution for non-Newtonian flow at $y = 0.4$ with fixed pseudoplastic parameter α_2 and absence of MHD interaction.

α_1	$x = 0$					$x = 0.75$				
	ADM	HAM	AE	Numerical	AE	ADM	HAM	AE	Numerical	AE
0.1	1.54892	1.54812	7.98×10^{-4}	1.55305	4.13×10^{-3}	2.01585	2.01574	1.01×10^{-4}	2.01386	2.05×10^{-3}
0.3	1.53836	1.53931	9.57×10^{-4}	1.54133	2.97×10^{-3}	1.98479	2.01483	3.00×10^{-2}	1.99247	7.61×10^{-3}
0.5	1.52797	1.52562	2.35×10^{-3}	1.52796	7.72×10^{-6}	1.95455	1.94774	6.81×10^{-3}	1.95651	1.94×10^{-3}
0.7	1.51775	1.51988	2.12×10^{-3}	1.51508	2.68×10^{-3}	1.92513	1.93396	8.82×10^{-3}	1.92693	1.76×10^{-3}
0.9	1.50772	1.50431	3.41×10^{-3}	1.50757	1.41×10^{-4}	1.89653	1.91473	1.82×10^{-2}	1.89572	8.34×10^{-4}

Table 5
Validation of numerical model against analytical solution for non-Newtonian flow at $y = 0.6$ with fixed pseudoplastic parameter α_2 and absence of MHD interaction.

α_1	$x = 0$					$x = 0.75$				
	ADM	HAM	AE	Numerical	AE	ADM	HAM	AE	Numerical	AE
0.1	1.42427	1.42443	1.64×10^{-4}	1.42467	4.05×10^{-4}	1.89119	1.92127	3.01×10^{-2}	1.89064	5.98×10^{-4}
0.3	1.41475	1.41711	2.35×10^{-3}	1.41531	5.62×10^{-4}	1.86119	1.90637	4.52×10^{-2}	1.86341	2.21×10^{-3}
0.5	1.40541	1.40178	3.63×10^{-3}	1.40438	1.03×10^{-3}	1.83199	1.80382	2.82×10^{-2}	1.83201	3.32×10^{-6}
0.7	1.39623	1.39471	1.52×10^{-3}	1.39391	2.32×10^{-3}	1.80361	1.82432	2.07×10^{-2}	1.79956	4.11×10^{-3}
0.9	1.38722	1.39252	5.30×10^{-3}	1.38775	5.35×10^{-4}	1.77603	1.82325	4.72×10^{-2}	1.77827	2.16×10^{-3}

Table 6
Validation of numerical model against analytical solution for non-Newtonian flow at $y = 0.8$ with fixed pseudoplastic parameter α_2 and absence of MHD interaction.

α_1	$x = 0$					$x = 0.75$				
	ADM	HAM	AE	Numerical	AE	ADM	HAM	AE	Numerical	AE
0.1	1.24352	1.24028	3.24×10^{-3}	1.24162	1.90×10^{-3}	1.71044	1.77292	6.25×10^{-2}	1.71095	4.53×10^{-4}
0.3	1.23695	1.24316	6.21×10^{-3}	1.23602	9.30×10^{-4}	1.68338	1.74197	5.86×10^{-2}	1.67806	5.39×10^{-3}
0.5	1.23051	1.22554	4.97×10^{-3}	1.22920	1.32×10^{-3}	1.65710	1.59585	6.13×10^{-2}	1.65393	3.21×10^{-3}
0.7	1.22421	1.22627	2.06×10^{-3}	1.22273	1.48×10^{-3}	1.63159	1.67011	3.85×10^{-2}	1.62178	9.90×10^{-3}
0.9	1.21804	1.21777	2.69×10^{-4}	1.21893	8.90×10^{-4}	1.60685	1.69267	8.58×10^{-2}	1.61094	4.04×10^{-3}

Table 7
Validation of numerical model against analytical solution for non-Newtonian flow at $y = 0$ with fixed pseudoplastic parameter α_2 and presence of MHD interaction.

α_1	$x = 0$					$x = 0.75$				
	ADM	HAM	AE	Numerical	AE	ADM	HAM	AE	Numerical	AE
0.1	1.15388	1.15263	1.24×10^{-3}	1.16333	9.45×10^{-3}	1.24598	1.24771	1.72×10^{-3}	1.24792	1.95×10^{-3}
0.3	1.15288	1.15134	1.54×10^{-3}	1.16221	9.32×10^{-3}	1.24317	1.24448	1.31×10^{-3}	1.24399	8.15×10^{-4}
0.5	1.15188	1.15004	1.85×10^{-3}	1.16108	9.19×10^{-3}	1.24036	1.24127	9.11×10^{-4}	1.23944	9.23×10^{-4}
0.7	1.15089	1.14874	2.15×10^{-3}	1.15995	9.07×10^{-3}	1.23755	1.23806	5.08×10^{-4}	1.23627	1.28×10^{-3}
0.9	1.14989	1.14744	2.45×10^{-3}	1.15883	8.94×10^{-3}	1.23475	1.23485	1.05×10^{-4}	1.23607	1.32×10^{-3}

Table 8
Validation of numerical model against analytical solution for non-Newtonian flow at $y = 0.2$ with fixed pseudoplastic parameter α_2 and presence of MHD interaction.

α_1	$x = 0$					$x = 0.75$				
	ADM	HAM	AE	Numerical	AE	ADM	HAM	AE	Numerical	AE
0.1	1.14791	1.14669	1.22×10^{-3}	1.15689	8.98×10^{-3}	1.24031	1.24193	1.62×10^{-3}	1.24154	1.23×10^{-3}
0.3	1.14691	1.14539	1.52×10^{-3}	1.15579	8.88×10^{-3}	1.23751	1.23872	1.21×10^{-3}	1.23812	6.07×10^{-4}
0.5	1.14592	1.14409	1.83×10^{-3}	1.15469	8.78×10^{-3}	1.23471	1.23551	7.99×10^{-4}	1.23331	1.40×10^{-3}
0.7	1.14492	1.14279	2.13×10^{-3}	1.15359	8.67×10^{-3}	1.23189	1.23229	3.90×10^{-4}	1.23061	1.28×10^{-3}
0.9	1.14393	1.14149	2.44×10^{-3}	1.15251	8.57×10^{-3}	1.22909	1.22907	1.82×10^{-5}	1.23043	1.34×10^{-3}

unidirectional steady flows produced by Maxwell fluids, Oldroyd 3-constant (Oldroyd-B) fluids, second-grade fluids, Oldroyd 6-constant and Oldroyd 8-constant fluids with $\alpha_1 = \alpha_2$ are equivalent to those of Newtonian fluids. It has been noted that as the modified Capillary's constant N_{ca_2} increases, the stronger viscous forces within the fluid make it resist thinning and spreading easily and delayed the separation point x_{sp} closer to the nip ($x = 0$). Also the resistance of the fluid prohibits to deform its spreading on the substrate results in a thinner final coating thickness ξ. In stark contrast to the dilatant parameter α_1, the pseudoplastic parameter α_2 has the opposite effect. Besides carefully selecting the relevant parameters, the results of the current research can also be directly compared to those of Zahid et al. [12] analysis, which is valid for a Newtonian fluid. In the upcoming research, people could leverage ADM and HAM to comprehend better and tackle problems in

Table 9
Validation of numerical model against analytical solution for non-Newtonian flow at $y = 0.4$ with fixed pseudoplastic parameter α_2 and presence of MHD interaction.

α_1	$x = 0$					$x = 0.75$				
	ADM	HAM	AE	Numerical	AE	ADM	HAM	AE	Numerical	AE
0.1	1.12991	1.12877	1.14×10^{-3}	1.13789	7.98×10^{-3}	1.19443	1.19533	9.07×10^{-4}	1.19606	1.63×10^{-3}
0.3	1.12893	1.12749	1.44×10^{-3}	1.13681	7.87×10^{-3}	1.19175	1.19223	4.80×10^{-4}	1.19053	1.22×10^{-3}
0.5	1.12796	1.12622	1.74×10^{-3}	1.13572	7.76×10^{-3}	1.18907	1.18912	5.39×10^{-5}	1.18635	2.72×10^{-3}
0.7	1.12699	1.12495	2.04×10^{-3}	1.13463	7.64×10^{-3}	1.18639	1.18602	3.73×10^{-4}	1.18447	1.92×10^{-3}
0.9	1.12602	1.12367	2.35×10^{-3}	1.13355	7.53×10^{-3}	1.18371	1.18291	7.99×10^{-4}	1.18427	5.59×10^{-4}

Table 10
Validation of numerical model against analytical solution for non-Newtonian flow at $y = 0.6$ with fixed pseudoplastic parameter α_2 and presence of MHD interaction.

α_1	$x = 0$					$x = 0.75$				
	ADM	HAM	AE	Numerical	AE	ADM	HAM	AE	Numerical	AE
0.1	1.09958	1.09863	9.53×10^{-4}	1.10578	6.19×10^{-3}	1.15341	1.15385	4.40×10^{-4}	1.15721	3.80×10^{-3}
0.3	1.098717	1.09748	1.23×10^{-3}	1.10481	6.09×10^{-3}	1.15101	1.15105	3.66×10^{-5}	1.15341	2.40×10^{-3}
0.5	1.09784	1.09633	1.51×10^{-3}	1.10383	5.99×10^{-3}	1.14862	1.14825	3.67×10^{-4}	1.14809	5.22×10^{-4}
0.7	1.09697	1.09519	1.79×10^{-3}	1.10286	5.89×10^{-3}	1.14622	1.14545	7.71×10^{-4}	1.14712	8.99×10^{-4}
0.9	1.09611	1.09404	2.07×10^{-3}	1.10189	5.79×10^{-3}	1.14383	1.14265	1.17×10^{-3}	1.14691	3.08×10^{-3}

Table 11
Validation of numerical model against analytical solution for non-Newtonian flow at $y = 0.8$ with fixed pseudoplastic parameter α_2 and presence of MHD interaction.

α_1	$x = 0$					$x = 0.75$				
	ADM	HAM	AE	Numerical	AE	ADM	HAM	AE	Numerical	AE
0.1	1.05641	1.05581	6.05×10^{-4}	1.06002	3.62×10^{-3}	1.09948	1.09953	5.70×10^{-5}	1.09677	2.71×10^{-3}
0.3	1.05581	1.05501	7.99×10^{-4}	1.05937	3.56×10^{-3}	1.09769	1.09743	2.61×10^{-4}	1.09295	4.73×10^{-3}
0.5	1.05522	1.05423	9.93×10^{-4}	1.05872	3.50×10^{-3}	1.09590	1.09532	5.80×10^{-4}	1.09806	2.16×10^{-3}
0.7	1.05463	1.05344	1.19×10^{-3}	1.05806	3.44×10^{-3}	1.09411	1.09321	8.98×10^{-4}	1.09785	3.74×10^{-3}
0.9	1.05404	1.05265	1.38×10^{-3}	1.05741	3.38×10^{-3}	1.09232	1.09111	1.22×10^{-3}	1.09763	5.31×10^{-3}

fluid mechanics problems [43], especially in RRC [44] and FRC [10,45] incorporating the heat transfer, entropy, slip and porosity effects.

Abbreviations

FRC	Forward roll coating
$\frac{D}{Dt}$	Material derivative
ADM	Adomian's Decomposition Method
U	Rolls' peripheral velocity
u	Velocity ratio
ρ	Density
ω	Rolls angular velocities
μ	Viscosity of the fluid
R	Radius of the roll
S	Extra stress tensor
H_0	Half the nip separation
AE	Absolute error

Research funding

This research article is subsided by National Natural Science Foundation of China (Grant No. 11971378) and Talent Project of Tianchi Doctoral Program in Xinjiang Uyger Autonomous Region of China.

CRediT authorship contribution statement

Muhammad Usman: Methodology, Software, Writing – original draft. **Yanren Hou:** Supervision, Funding acquisition. **Fateh Ali:** Conceptualization. **Muhammad Zahid:** Writing – review & editing. **Muhammad Afzal Rana:** Writing – review & editing.

Declaration of competing interest

The authors declare the following financial interests/personal relationships which may be considered as potential competing interests: Yanren Hou reports financial support was provided by National Natural Science Foundation of China. If there are other authors, they declare that they have no known competing financial interests or personal relationships that could have appeared to influence the work reported in this paper.

Data availability

No data was used for the research described in the article.

Appendix A. Analysis of Adomian's decomposition method

The decomposition method can be briefly explained using the following differential equation:

$$Lu + Nu = g, \tag{67}$$

where L signifies a linear operator, N denotes a non-linear operator, g serves as the source term, and $u = u(y)$ only. The result of applying L^{-1} to Eq. (67) can be represented as follows:

$$u = f + L^{-1}g - L^{-1}Nu, \tag{68}$$

where the term generated through the solution of the homogeneous equation is denoted by the function f.

$$Lu = 0, \tag{69}$$

encompassing the constants of integration. During the decomposition procedure, the solution $u(y)$ is represented in the form of a series of decomposition terms:

$$u(y) = \sum_{n=0}^{\infty} u_n(y). \tag{70}$$

In Eq. (68), the polynomial series of Adomian's decomposition contains a nonlinear term denoted by $Nu(y)$. These terms can be defined as follows:

$$N_1 u(y) = \sum_{n=0}^{\infty} A_n, \tag{71}$$

$$N_2 u(y) = \sum_{n=0}^{\infty} B_n, \tag{72}$$

where A_n and B_n represent the Adomian's polynomials utilized in this particular context. The provided formula can be used to calculate each non-linear term.

$$A_n = B_n = \frac{1}{n!}\frac{d^m}{d\lambda^m}\left[N\left(\sum_{i=0}^{\infty} u_i\right)\right]_{\lambda=0}, \quad n = 0, 1, 2, 3, \ldots. \tag{73}$$

The third order polynomials of Adomian's decomposition, A_n and B_n are expressed as follows:

$$\begin{aligned}
A_0 &= \left(\frac{du_0}{dy}\right)^2\left(\frac{d^2u_0}{dy^2}\right),\\
B_0 &= \left(\frac{du_0}{dy}\right)^2,\\
A_1 &= 2\left(\frac{du_0}{dy}\right)\left(\frac{d^2u_0}{dy^2}\right)\left(\frac{du_1}{dy}\right) + \left(\frac{du_0}{dy}\right)^2\left(\frac{d^2u_1}{dy^2}\right),\\
B_1 &= 2\left(\frac{du_0}{dy}\right)\left(\frac{du_1}{dy}\right),\\
A_2 &= \left(\frac{du_1}{dy}\right)^2\left(\frac{d^2u_0}{dy^2}\right) + 2\left(\frac{du_0}{dy}\right)\left(\frac{d^2u_1}{d^2y}\right)\left(\frac{du_1}{dy}\right)\\
&\quad + 2\left(\frac{du_0}{dy}\right)\left(\frac{d^2u_0}{d^2y}\right)\left(\frac{du_2}{dy}\right) + \left(\frac{du_0}{dy}\right)^2\left(\frac{d^2u_2}{dy^2}\right),\\
B_2 &= \left(\frac{du_1}{dy}\right)^2 + 2\left(\frac{du_0}{dy}\right)\left(\frac{du_2}{dy}\right),\\
A_3 &= 2\left(\frac{du_1}{dy}\right)\left(\frac{d^2u_0}{d^2y}\right)\left(\frac{du_2}{dy}\right) + \left(\frac{du_1}{dy}\right)^2\left(\frac{d^2u_1}{dy^2}\right)\\
&\quad + 2\left(\frac{du_0}{dy}\right)\left(\frac{d^2u_2}{d^2y}\right)\left(\frac{du_1}{dy}\right)\\
&\quad + 2\left(\frac{du_0}{dy}\right)\left(\frac{d^2u_1}{d^2y}\right)\left(\frac{du_2}{dy}\right) + 2\left(\frac{du_0}{dy}\right)\left(\frac{d^2u_0}{d^2y}\right)\left(\frac{du_3}{dy}\right)\\
&\quad + \left(\frac{du_0}{dy}\right)^2\left(\frac{d^2u_3}{d^2y}\right),\\
B_3 &= 2\left(\frac{du_0}{dy}\right)\left(\frac{du_3}{dy}\right) + 2\left(\frac{du_1}{dy}\right)\left(\frac{du_2}{dy}\right),\\
&\vdots
\end{aligned} \tag{74}$$

as far as we establish

$$u_0 = f + L^{-1}g, \tag{75}$$

and make use of Eqs. (73)–(74) in (68), the Eq. (75) becomes:

$$\sum_{n=0}^{\infty} u_n(y) = u_0 - L^{-1}\left(\sum_{n=0}^{\infty}(A_n + B_n)\right), \tag{76}$$

which gives

$$\begin{aligned}
u_1(y) &= -L^{-1}\left(A_0 + B_0\right),\\
u_2(y) &= -L^{-1}\left(A_1 + B_1\right),\\
u_3(y) &= -L^{-1}\left(A_2 + B_2\right),\\
&\vdots\\
u_{n+1}(y) &= -L^{-1}\left(A_n + B_n\right).
\end{aligned} \tag{77}$$

By combining all the terms, the series solution can be represented in the form:

$$u(y) = \sum_{n=0}^{\infty} u_n. \tag{78}$$

where $u_1, u_2, u_3, \ldots$ are determined using Eq. (78).

Appendix B. Analysis of homotopy analysis method

To obtain a complete analytical and uniformly valid solution, we use the homotopy analysis method for the given problem.

$$\mathcal{L}[\bar{u}(y;p)] = \frac{\partial^2\bar{u}(y;p)}{\partial y^2} - m^2\bar{u}(y;p), \tag{79}$$

as an additional linear operator, where the embedding parameter $p \in [0, 1]$ is present. Let us formulate the equation for zeroth-order deformation as

$$\begin{aligned}
&(1-p)\mathcal{L}[\bar{u}(y;p) - u_0(y)]\\
&\quad = p\hbar\left[\frac{\partial^2\bar{u}(y;p)}{\partial y^2} + \left\{(3\alpha_1 - \alpha_2) + \alpha_1\alpha_2\left(\frac{\partial\bar{u}(y;p)}{\partial y}\right)^2\right\}\right.\\
&\quad\quad \times\left(\frac{\partial\bar{u}(y;p)}{\partial y}\right)^2\frac{\partial^2\bar{u}(y;p)}{\partial y^2}\\
&\quad\quad \left. - \left(m^2\bar{u}(y;p) + \frac{d\hat{p}}{dx}\right)\left\{1 + \alpha_2\left(\frac{\partial\bar{u}(y;p)}{\partial y}\right)^2\right\}^2\right],
\end{aligned} \tag{80}$$

with the appropriate boundary conditions

$$\bar{u}(h;p) = 1, \quad \frac{d\bar{u}(0;p)}{dy} = 0. \tag{81}$$

where $\hbar \neq 0$ is a auxiliary parameter.

It is obvious that the Eqs. (80) and (81) have a solution when $p = 0$

$$\bar{u}(y;0) = u_0(y). \tag{82}$$

Eqs. (80) and (81) are identical to Eqs. (36) and (37) if $p = 1$

$$\bar{u}(y;1) = u(y). \tag{83}$$

Thereby further, the change in p from 0 to 1 is equivalent to the continuous variation of $\bar{u}(y;p)$ from the initial approximation $u_0(y)$ to the unknown outcome $u(y)$ of Eqs. (36) and (37).

Suppose that the deformation $\bar{u}(y;p)$ controlled by Eqs. (80) and (81) is sufficiently uniform.

$$u_0^{[k]}(y) = \left.\frac{\partial^k\bar{u}(y;p)}{\partial p^k}\right|_{p=0}, \qquad (k \geq 1) \tag{84}$$

namely, the kth-order deformation derivative exists. Expanding $\bar{u}(y;p)$ in power series of the embedding parameter p using Eq. (82) is straightforward:

$$\bar{u}(y;p) = u_0(y) + \sum_{k=1}^{+\infty} u_k(y)p^k, \tag{85}$$

where

$$u_k(y) = \left.\frac{1}{k!}\frac{\partial^k\bar{u}(y;p)}{\partial p^k}\right|_{p=0}, \qquad (k \geq 1). \tag{86}$$

It is important to note that the deformation equation of order zero, as presented in Eq. (80), includes an auxiliary parameter $\hbar$ that is non-zero. The convergence rate and region of the series (85) are impacted by the dependence of $\bar{u}(y;p)$ and $u_k(y)$ on the auxiliary parameter $\hbar$. Assuming $\hbar$ is properly chosen, series (85) converges at $p = 1$. As a result of Eqs. (83) and (85), we can establish a connection.

$$u(y) = u_0(y) + \sum_{k=1}^{+\infty} u_k(y). \tag{87}$$

Differentiating the zeroth-order deformation Eqs. (80) and (81)k times with respect to p, dividing by $k!$, and setting $p = 0$, gives the kth-order deformation problem due to definition (86).

$$\begin{aligned}
&\mathcal{L}[u_k(y) - \chi_k u_{k-1}(y)] =\\
&\hbar\left[\begin{array}{l}
u''_{k-1} + \sum_{n=0}^{k-1} u''_{k-n-1}\sum_{i=0}^{n} u'_{n-1}\left((3\alpha_1 - \alpha_2)u'_i + \alpha_1\alpha_2\sum_{j=0}^{i} u'_{i-j}\sum_{r=0}^{j} u'_{j-r}u'_r\right)\\
- m^2\left\{u_{k-1} + \alpha_2\sum_{n=0}^{k-1} u_{k-n-1}\sum_{i=0}^{n} u'_{n-i}\left(2u'_i + \alpha_2\sum_{j=0}^{i} u'_{i-j}\sum_{r=0}^{j} u'_{j-r}u'_r\right)\right\}\\
- \alpha_2\frac{d\hat{p}}{dx}\sum_{n=0}^{k-1} u'_{k-n-1}\left(2u'_n + \alpha_2\sum_{i=0}^{n} u'_{n-i}\sum_{j=0}^{i} u'_{i-j}u'_j\right)
\end{array}\right],
\end{aligned} \tag{88}$$

$$u_k(h) = 1, \quad \frac{du_k(0)}{dy} = 0. \tag{89}$$

Appendix C. Algorithm and procedure to execute Finite Difference Algorithm with SOR

Algorithm 1 Finite Difference Algorithm with SOR

Require: Initial guess $\mathbf{u}^{(0)}$, relaxation factor τ, tolerance ϵ
Ensure: Approximate solution $\mathbf{u}$

1: $n \leftarrow 0$
2: **while** $\|\mathbf{u}^{(n+1)} - \mathbf{u}^{(n)}\| > \epsilon$ **do**
3: **for** $i = 1$ to $N_x - 1$ **dof**
4: $u_i^{(n+1)} \leftarrow \frac{1}{2}(u_{i+1}^{(n)} + u_{i-1}^{(n+1)}) + 2\tau^2 \left[\beta + \alpha_1\alpha_2 \frac{1}{4\tau^2}\left(u_{i+1}^{(n)} - u_{i-1}^{(n+1)}\right)^2\right] \times \left(\frac{1}{4\tau^2}\left(u_{i+1}^{(n)} - u_{i-1}^{(n+1)}\right)^2\right)\left(\frac{1}{4\tau^2}u_{i+1}^{(n)} - 2u_i^{(n)} + u_{i-1}^{(n+1)}\right) + \left(m^2 u_i^{(n)} + \frac{dP}{dx}\right)\left[1 + \alpha_2\left(\frac{1}{4\tau^2}\left(u_{i+1}^{(n)} - u_{i-1}^{(n+1)}\right)^2\right)\right]^2$
5: **end for**
6: $n \leftarrow n + 1$
7: **end while**
8: $\mathbf{u} \leftarrow \mathbf{u}^{(n)}$

Procedure to execute Finite Difference Algorithm with SOR:

1. **Discretization**: The central difference formulas of first and second order derivatives with respect to y are approximated as:

$$\frac{du}{dy} \approx \frac{u_{i+1} - u_{i-1}}{2\tau} \tag{90}$$

$$\frac{d^2u}{dy^2} \approx \frac{u_{i+1} - 2u_i + u_{i-j}}{\tau^2} \tag{91}$$

2. **Initialization**: Set initial guess $u^{(0)}(y)$, relaxation factor $\tau \in (0, 1]$, and convergence tolerance $\epsilon = 10^{-8}$.
3. **Iteration**: Repeat until the solution converges within the tolerance:
   - Sweep through interior grid points ($i = 1$ to $N_y - 1$)
   - Update each grid point using the SOR formula by combine current value, weighted average of neighboring values, and source term and over-relax using the relaxation factor τ (controls the degree of overshooting; crucial for optimal performance).
4. **Solution**: Assign the converged solution to u.

Appendix D. Auxiliary constants

Below, we present values for various constants that exist in sections (Sections "Adomian's Decomposition Method (ADM)" and "Homotopy Analysis Method (HAM)"):

$$l_1 = -\frac{243\left(\xi_0 - h\right)^5 \alpha_2^2}{5h^{15}} + \frac{243\alpha_1\alpha_2\left(\xi_0 - h\right)^5}{5h^{15}},$$

$$l_2 = -\frac{27\left(\xi_0 - h\right)^3 \alpha_2}{h^9} + \frac{27\alpha_1\left(\xi_0 - h\right)^3}{h^9},$$

$$l_3 = \frac{1}{4}l_2,$$

$$l_4 = \frac{1}{6}l_1,$$

$$\beta = 3\alpha_1 - \alpha_2.$$

References

[1] Truesdell C, Noll W, Truesdell C, Noll W. The non-linear field theories of mechanics. Springer; 1965.
[2] Hintermaier J, White R. The splitting of a water film between rotating rolls. TAPPI J 1965;48(11):617–25.
[3] Greener J, Middleman S. Reverse roll coating of viscous and viscoelastic liquids. Ind Eng Chem Fundam 1981;20(1):63–6.
[4] Jang J-Y, Chen P-Y. Reverse roll coating flow with non-Newtonian fluids. Commun Comput Phys 2009;6(3):536.
[5] Balzarotti F, Rosen M. Systematic study of coating systems with two rotating rolls. Lat Am Appl Res 2009;39(2):99–104.
[6] Belblidia F, Tamaddon-Jahromi H, Echendu S, Webster M. Reverse roll-coating flow: A computational investigation towards high-speed defect free coating. Mech Time-Dependent Mater 2013;17:557–79.
[7] Hayat T, Khan M, Asghar S. Homotopy analysis of MHD flows of an Oldroyd 8-constant fluid. Acta Mech 2004;168(3–4):213–32.
[8] Ellahi R, Hayat T, Mahomed F, Zeeshan A. Exact solutions for flows of an Oldroyd 8-constant fluid with nonlinear slip conditions. Commun Nonlinear Sci Numer Simul 2010;15(2):322–30.
[9] S. B. Flow of an Oldroyd 8-constant fluid in a convergent channel. Acta Mech 2001;148(1–4):117–27.
[10] Usman M, Hou Y, Zahid M, Ali F, Rana MA. Analytical study of viscoelastic fluid during forward roll coating process under lubrication approximation theory. Internat J Modern Phys B 2023;2450287.
[11] Usman M, Hou Y, Zahid M, Ali F, Rana MA. Soft computing through neural network based on levenberg-marquardt for numerical treatment of steady flow of Oldroyd 4-constant fluid between two rolls. Internat J Modern Phys C 2023. http://dx.doi.org/10.1142/S0129183124500712.
[12] Zahid M, Zafar M, Rana M, Rana M, Lodhi M. Numerical analysis of the forward roll coating of a rabinowitsch fluid. J Plastic Film Sheet 2020;36(2).
[13] Daprà I, Scarpi G. Perturbation solution for pulsatile flow of a non-Newtonian Williamson fluid in a rock fracture. Int J Rock Mech Min Sci 2007;44(2):271–8.
[14] Zahid M, Siddique I, Ali R. Coating of a viscoplastic material onto a moving porous web during forward roll coating process: A theoretical study. J Plastic Film Sheet 2023;39(1):19–51.
[15] Sarpkaya T. Flow of non-Newtonian fluids in a magnetic field. AIChE J 1961;7(2):324–8.
[16] Hayat T, Sajid M. Homotopy analysis of MHD boundary layer flow of an upper-convected Maxwell fluid. Internat J Engrg Sci 2007;45(2–8):393–401.
[17] Wang Y, Hayat T, Hutter K. Magnetohydrodynamic flows of an Oldroyd 8-constant fluid in a porous medium. Canad J Phys 2004;82(11):965–80.
[18] Khan M, Hayat T, Ayub M. Numerical study of partial slip on the MHD flow of an Oldroyd 8-constant fluid. Comput Math Appl 2007;53(7):1088–97.
[19] Ellahi R, Hayat T, Javed T, Asghar S. On the analytic solution of nonlinear flow problem involving Oldroyd 8-constant fluid. Math Comput Model 2008;48(7–8):1191–200.
[20] Hamid A, Naveen Kumar R, Punith Gowda R, Varun Kumar R, Khan SU, Ijaz Khan M, et al. Impact of hall current and homogenous–heterogenous reactions on MHD flow of GO-MoS2/water (H2O)-ethylene glycol (C2H6O2) hybrid nanofluid past a vertical stretching surface. Waves Random Complex Media 2021;1–18.
[21] Raza A, Khan SU, Al-Khaled K, Khan MI, Haq AU, Alotaibi F, et al. A fractional model for the kerosene oil and water-based casson nanofluid with inclined magnetic force. Chem Phys Lett 2022;787:139277.
[22] Raja MAZ, Shoaib M, Tabassum R, Khan MI, Gowda RP, Prasannakumara B, et al. Intelligent computing for the dynamics of entropy optimized nanofluidic system under impacts of MHD along thick surface. Internat J Modern Phys B 2021;35(26):2150269.
[23] Abel S, Prasad K, Mahaboob A. Buoyancy force and thermal radiation effects in MHD boundary layer visco-elastic fluid flow over continuously moving stretching surface. Int J Therm Sci 2005;44(5):465–76.
[24] Chen C-H. On the analytic solution of MHD flow and heat transfer for two types of viscoelastic fluid over a stretching sheet with energy dissipation, internal heat source and thermal radiation. Int J Heat Mass Transfer 2010;53(19–20):4264–73.
[25] Akbar NS, Ebaid A, Khan Z. Numerical analysis of magnetic field effects on Eyring-Powell fluid flow towards a stretching sheet. J Magnet Magnet Mater 2015;382:355–8.
[26] Khan Z, Ur Rasheed H, Ullah M, Gul T, Jan A. Analytical and numerical solutions of Oldroyd 8-constant fluid in double-layer optical fiber coating. J Coat Technol Res 2019;16:235–48.
[27] Aich W, Abbas T, Sewify GH, Sadiq MN, Khan SU, Bilal M, et al. Comparative numerical and analytical computations for magnetized pseudoplastic materialwith roll-coating applications. Alex Eng J 2023;79:538–44.
[28] Farooq S, Khan MI, Riahi A, Chammam W, Khan WA. Modeling and interpretation of peristaltic transport in single wall carbon nanotube flow with entropy optimization and Newtonian heating. Comput Methods Programs Biomed 2020;192:105435.

[29] Chu Y-M, Al-Khaled K, Khan N, Khan MI, Khan SU, Hashmi MS, et al. Study of Buongiorno's nanofluid model for flow due to stretching disks in presence of gyrotactic microorganisms. Ain Shams Eng J 2021;12(4):3975–85.
[30] Li S, Ali F, Zaib A, Loganathan K, Eldin SM, Ijaz Khan M. Bioconvection effect in the Carreau nanofluid with Cattaneo–Christov heat flux using stagnation point flow in the entropy generation: Micromachines level study. Open Phys 2023;21(1):20220228.
[31] Liu H, Xu K, Zhu T, Ye W. Multiple temperature kinetic model and its applications to micro-scale gas flows. Comput & Fluids 2012;67:115–22.
[32] Adomian G. A review of the decomposition method and some recent results for nonlinear equations. Math Comput Modelling 1990;13(7):17–43.
[33] Wazwaz A-M. Adomian decomposition method for a reliable treatment of the Bratu-type equations. Appl Math Comput 2005;166(3):652–63.
[34] Wazwaz A-M. Adomian decomposition method for a reliable treatment of the Emden–Fowler equation. Appl Math Comput 2005;161(2):543–60.
[35] Zeeshan K, Islam S, Shah R, Khan I, Gul T, Gaskel P. Double-layer optical fiber coating analysis by withdrawal from a bath of Oldroyd 8-constant fluid. J Appl Environ Biol Sci 2015;5(2):36–51.
[36] Liao SJ. On the analytic solution of magnetohydrodynamic flows of non-Newtonian fluids over a stretching sheet. J Fluid Mech 2003;488:189–212.
[37] Liao SJ. On the homotopy analysis method for nonlinear problems. Appl Math Comput 2004;147(2):499–513.
[38] Rossow VJ. On flow of electrically conducting fluids over a flat plate in the presence of a transverse magnetic field. Technical report, 1958.
[39] Bird RR, Armstrong RC, Hassager O. Dynamics of polymeric liquids, volume 1: fluid mechanics. Wiley; 1987.
[40] Huilgol RR. Continuum mechanics of viscoelastic liquids. Hindustan Pub. Corp. and Halsted Press; 1975, URL https://cir.nii.ac.jp/crid/1130000795865011072.
[41] Greener J, Middleman S. Theoretical and experimental studies of the fluid dynamics of a two-roll coater. Ind Eng Chem Fundam 1979;18(1):35–41.
[42] Cherruault Y, Adomian G. Decomposition methods: A new proof of convergence. Math Comput Modelling 1993;18(12):103–6.
[43] Waseem W, Sulaiman M, Islam S, Kumam P, Nawaz R, Raja MAZ, et al. A study of changes in temperature profile of porous fin model using cuckoo search algorithm. Alex Eng J 2020;59(1):11–24.
[44] Ali F, Hou Y, Zahid M, Rana M, Kumam P, Kanwal M, et al. Perturbation based analytical and numerical solutions of non-Newtonian differential equation during reverse roll coating process under lubrication approximation theory. Phys Scr 2022;97(11):115203.
[45] Ali F, Hou Y, Zahid M, Rana M, Kumam P, Sitthithakerngkiet K. Numerical analysis of heat transfer and magnetohydrodynamic flow of viscoelastic Jeffery fluid during forward roll coating proces. Heat Transf 2023.